
Consistency of mechanistic causal discovery in continuous-time using Neural ODEs

A PREPRINT

Alexis Bellot^{1,2} Kim Branson⁴ Mihaela van der Schaar^{1,2,3}

¹University of Cambridge, ²The Alan Turing Institute, ³UCLA, ⁴GlaxoSmithKlein
 abellot@turing.ac.uk

November 17, 2021

Abstract

The discovery of causal mechanisms from time series data is a key problem in fields working with complex systems. Most identifiability results and learning algorithms assume the underlying dynamics to be discrete in time. Comparatively few, in contrast, explicitly define causal associations in infinitesimal intervals of time, independently of the scale of observation and of the regularity of sampling. In this paper, we consider causal discovery in continuous-time for the study of dynamical systems. We prove that for vector fields parameterized in a large class of neural networks, adaptive regularization schemes consistently recover causal graphs in systems of ordinary differential equations (ODEs). Using this insight, we propose a causal discovery algorithm based on penalized Neural ODEs that we show to be applicable to the general setting of irregularly-sampled multivariate time series and to strongly outperform the state of the art.

1 Introduction

This paper deals with the discovery of the underlying causal mechanism from a combination of non-experimental (e.g. observational) temporal data and qualitative assumptions about the nature of causality in dynamical systems. This problem is an important aspect of scientific discovery, especially for fields involved with complex systems, such as biology [81, 60, 26] and climate science [7, 61, 70], for which extensive experimentation is difficult. For example, oncologists may be interested in the signalling pathways of genes over-expressed in cancerous cells even though interventions may not be immediately feasible, e.g. as described by Sanchez-Vega et al. [72]. For these problems, the ordering and the timing of observations can serve as axioms to ground the nature of causality without explicitly relying on an interventionist account [56]. Time itself can be used to define a fundamental asymmetry between cause and effect, distinguishing between direct effects (that occur over infinitesimal time intervals not mediated by other variables in the system) and indirect effects (that necessarily occur over longer time frames). Causality in this interpretation unfolds in a continuous manner over time, tightly linked with the underlying, infinitesimal dynamics of the processes involved in the system.

This continuous-time view of causation is sometimes called *mechanistic* – causal claims are claims about the existence of a mechanism or process that mediates events at one time with events at a later time (see e.g. Williamson et al. [84] for an introduction and [71, 28, 29, 47] for essays on the philosophical basis of mechanistic causality)¹. One consequence of this interpretation for modelling causal relations is that causation should be formalised as the state of variables (e.g. $\mathbf{x}(t) \in \mathbb{R}^d$) contemporaneously influencing the rate of change of the same or other variables (e.g. $d\mathbf{x}(t)$),

$$d\mathbf{x}(t) = \mathbf{f}(\mathbf{x}(t))dt, \quad \mathbf{x}(0) = \mathbf{x}_0, \quad t \in [0, T]. \quad (1)$$

¹In particular, mechanistic causality does not appeal to interventions, e.g. as defined by Huw Price [59], or counterfactuals, e.g. as in the account of David Lewis [43], which suggests conceptual distinctions with formalisms involving structural equations models (which may be understood as a set of observational, distributional and counterfactual distributions, see e.g. [56]) and potential outcome models, see e.g. [67].

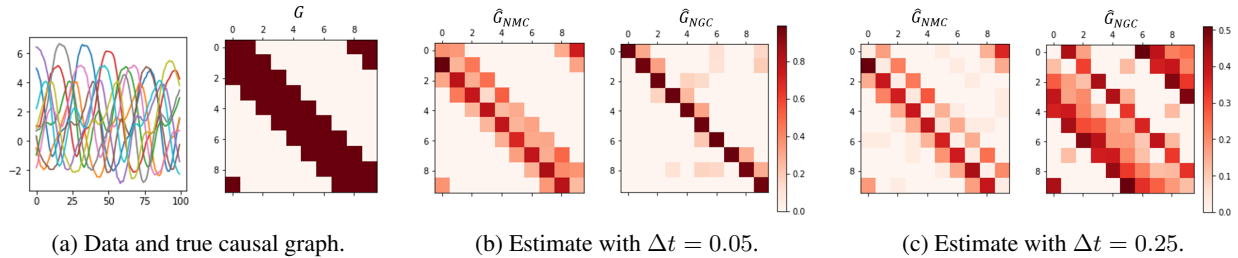


Figure 1: Visual comparison of the true and learned causal adjacency matrices (defined in section 3.1) of a 10-variable Lorenz system (see section 4.1). \hat{G}_{NMC} (the proposed approach) and \hat{G}_{NGC} (Neural Granger Causality [80]) are estimates of continuous and discrete-time algorithms respectively. Panel (a) shows a data sample and the true adjacency matrix, panel (b) shows estimates with higher frequency of observation ($\Delta t = t_i - t_{i-1} = 0.05$) and panel (c) with lower frequency of observation ($\Delta t = 0.25$). (The heat scale gives the strength of estimated causal interactions.)

The defining characteristic, as described by Iwasaki et al. [37], is that all causation across time is due to a derivative (e.g., dx) causing a change in its integral (e.g., x). All other causation is contemporaneous, occurring between two variables on a time-scale that is smaller than the time-step of observation. For instance, considering infinitesimal differentials dt and $dx = \mathbf{x}(t + dt) - \mathbf{x}(t)$ it is clear from $\mathbf{x}(t + dt) \approx \mathbf{x}(t) + \mathbf{f}(\mathbf{x}(t)) \cdot dt$ that the immediate future of each entry in \mathbf{x} is causally defined in terms of its present values and those entries of the vector $\mathbf{x}(t)$ involved in its dynamics \mathbf{f} .

The problem we tackle in this paper is to recover consistently the causal mechanism from data in the form of a causal graph \mathcal{G} and associated adjacency matrix $G \in \{0, 1\}^{d \times d}$ given by the sparsity pattern of \mathbf{f} without however making strong assumptions on the domain of \mathbf{f} or the pattern of observations.

1.1 Causal discovery in continuous-time

Temporal data often only loosely relates to the underlying dynamical system. We consider $\mathbf{x} : [0, T] \rightarrow \mathcal{X}^d \subset \mathbb{R}^d$ to be partially observed up to measurement noise on a sequence of n irregular time points $0 \leq t_1 < \dots < t_n \leq T$,

$$\mathbf{y}_i = \mathbf{x}(t_i) + \epsilon_i, \quad \epsilon = (\epsilon_1, \dots, \epsilon_n) \sim \mathcal{N}(0, \Sigma_n), \quad i = 1, \dots, n, \quad (2)$$

with a potentially significant dependency structure between neighbouring observations depending on the time interval between them. A number of remarks at this point will be useful to contextualize our contribution and emphasize distinctions with prior work.

- Observed data is systematically subsampled. Associations in discrete-time in general do not correspond to causality and may be highly dependent on the interval between observations, see e.g. example 2 in [69] and [31, 16]. The same subsampled discrete model may disaggregate to several continuous models, which are observationally equivalent at the subsampled frequency. Figure 1 provides an example to complement this point, noting also, as we will describe, that an explicitly continuous-time estimation method may be much better behaved. As a consequence as well, the realm of problems that involve irregularly-sampled data are out of scope in discrete-time in general but potentially tractable in continuous-time.
- An explicitly mechanistic (continuous-time) interpretation of causality is relatively unexplored. With this approach, arguments on identifiability of causal relationships are based on the premise that with enough data, one can consistently estimate the dependencies between implicit derivatives and the inferred state of variables at each time (rather than relying on a favourable observation sampling rate). Irregular sampling does not, in principle, alter this strategy as long as we can rule out pathological cases of subsampling that would prevent us from estimating the dependencies given by the (latent) vector field \mathbf{f} consistently.
- Samples $(\mathbf{y}_1, \dots, \mathbf{y}_n)$ are not independent which can (and does) increase the sample complexity. An increasing sample frequency will produce an increasing number of distinct samples. However, samples become more dependent, and intuitively one expects that there is limited information to be harnessed from a given time interval $[0, T]$.

1.2 Contributions

Our results formalize these intuitions. We propose a mechanistic account of causality for dynamical systems by explicitly modelling the (latent) vector field \mathbf{f} in a system of ordinary differential equations (ODEs). We prove that

for vector fields \mathbf{f} parameterized by analytic neural networks, the graph \hat{G} derived from the solution $\hat{\mathbf{f}}$ of a penalized optimization problems of the form,

$$\arg \min_{\mathbf{f}_\theta} \frac{1}{n} \sum_{i=1}^n \|\mathbf{y}_i - \mathbf{x}(t_i)\|_2^2, \quad \text{subject to } \rho_{n,T}(\mathbf{f}_\theta) \leq \eta \quad \text{and} \quad d\mathbf{x}(t) = \mathbf{f}_\theta(\mathbf{x}(t))dt, \quad (3)$$

consistently estimates G . $\rho_{n,T}(\mathbf{f}_\theta)$ is a constraint on the parameter space of \mathbf{f}_θ . The sample complexity of this problem depends both on the frequency of sampling n as well as on the time horizon T . We propose an instantiation of this method using Neural ODEs, as proposed by Chen et al. [10], showing empirically that mechanistic causality can be inferred consistently in a large range of settings involving irregularly-sampled multivariate time series with non-linear dependencies.

2 Related work

A substantial amount of work devoted to graphical modelling has considered the analysis of penalized least squares and its variants, most prominently in the high-dimensional regression literature with *i.i.d* data, see e.g. [25, 91, 90]. Closely related to our results are a number of extensions that have considered parameter identification in neural networks, using for instance a sparse one-to-one linear layers [45], group lasso constraints of the input layer of parameters [89] and input to output residual connections [42]. For a large class of neural networks Dinh et al. [20] proved the consistency of adaptive regularization methods. The distinction with our formalism in (3) is that the observations are not corrupted by *i.i.d*. noise (since successive samples are correlated) and therefore standard concentration inequalities are not sufficient.

Learning graphical models with dependent noise terms is also a topic of significant literature in the context of Granger causality, proposed by Clive Granger in [32] and also popularized by Christopher Sims [77] within autoregressive models. Various authors have considered the consistency of penalized vector autoregression models and proposed tests of Granger causality using parameter estimates in these models, see e.g. [53, 39, 3, 13], and extended some of these approaches to models of neural networks, see e.g. [80, 38, 48] (without however proving consistency of inference). Methods exist also using conditional independence tests such as those given by Runge et al. [68] and transfer entropy principles originating in Thomas Schreiber [73]. The conceptual, statistical and graphical contrasts between mechanistic and Granger accounts of causality are substantial and are more thoroughly discussed in the Appendix.

In the context of differential equations, penalized regression has been explored using two-stage collocation methods, first proposed by Varah et al. [82], by which derivatives are estimated on smoothed data and subsequently regressed on observed samples for inference. The consistency of parameter estimates has been established for linear models in parameters, as done for example in [64, 11, 86, 8]. From a modelling perspective, our approach in contrast is end-to-end, coupling the estimation of the underlying paths \mathbf{x} and the vector field \mathbf{f} . Graphical modelling has also been considered for linear stochastic differential equations by Bento et al. [5]. Similarly to the discrete-time literature, proposals exist for recovering non-linear vector fields via neural networks (see e.g. [63]) and Gaussian processes (see e.g. [33, 83]) but we are not aware of any identifiability guarantees.

3 Mechanistic Causal Discovery

We consider the underlying structure of an evolving process to be described by a multivariate dynamical system of d distinct deterministic processes $\mathbf{x} = (x_1, \dots, x_d) : [0, T] \rightarrow \mathcal{X}^d$ with each instantiation in time $x_j(t)$ for $j = 1, \dots, d$ and $t > 0$ defined in a bounded open set $\mathcal{X} \subset \mathbb{R}$. We assume that there exist functions $f_1, \dots, f_d \in \mathcal{F}$ such that $f_j : \mathcal{X}^d \rightarrow \mathbb{R}$ and,

$$\frac{d}{dt}x_j(t) = f_j(\mathbf{x}(t)), \quad \mathbf{x}(t_0) = \mathbf{x}_0, \quad t \in [0, T], \quad (4)$$

with \mathcal{F} defined as the space of analytic feed-forward neural networks with sets of parameters $\theta \in \Theta$ defined in bounded, real-valued intervals. It will be useful to define each layer of each network precisely. Let $A_1^j \in \mathbb{R}^{d \times h}$ denote the $d \times h$ weight matrix (we omit biases for clarity) in the input layer of $f_j, j = 1, \dots, d$. Let $A_m^j \in \mathbb{R}^{h \times h}$, for $m = 2, \dots, M-1$, denote the weight matrix of each hidden layer, and let $A_M^j \in \mathbb{R}^{h \times 1}$ be the $h \times 1$ dimensional output layers of each sub-network such that,

$$f_j(\mathbf{Y}) := \phi(\dots \phi(\phi(\mathbf{Y}A_1^j)A_2^j) \dots)A_M^j, \quad j = 1, \dots, d, \quad (5)$$

where $\phi(\cdot)$ is an analytic activation function (e.g. tanh, sigmoid, arctan, softplus, etc.) and $\mathbf{Y} \in \mathbb{R}^{n \times d}$ is the input data. Write $\mathbf{f}_{\theta_0} = (f_1, \dots, f_d)$ for the true underlying vector field, parameterized by a set of parameter values θ_0 .

The data \mathbf{Y} , in practice, is a partial, noisy sequence of observations of \mathbf{x} such that,

$$\mathbf{y}_i = \mathbf{x}(t_i) + \epsilon_i, \quad i = 1, \dots, n, \quad \epsilon = (\epsilon_1, \dots, \epsilon_n) \sim \mathcal{N}(0, \Sigma_n), \quad (6)$$

made on time points $0 \leq t_1 < \dots < t_n \leq T$ with a dependency structure encoded in $\Sigma_n \in \mathbb{R}^{n \times n}$. We assume the data to be normalized, i.e. diagonal elements of Σ_n to be equal to 1. The closer in time two observations are the more closely correlated we can expect them to be. With this system, for any inference to have a causal interpretation and estimation to be viable in practice we make a number of assumptions².

Assumption 1 (Causal sufficiency). *A system of processes \mathbf{x} is causally sufficient if no other (unobserved) process interacts with any of the observed ones.*

Time points at which observations are made are themselves assumed stochastic, driven a priori by a temporal point process with intensity $\lim_{dt \rightarrow 0} Pr(\text{Observation in } [t, t + dt] | \mathcal{H}_t) > 0$ for any $t > 0$ with respect to a filtration \mathcal{H}_t . Perfectly homogeneous and systematic subsampling has measure zero under this probability model and in principle will enable us to infer local conditional independencies arbitrarily well with increasing sample size.

Assumption 2 (Stochastic observation times). *Observations times (t_1, \dots, t_n) are sampled from a temporal point process with positive intensity.*

Definition 1 (Causal significance). *A process x_k is said to be causally significant for a process x_j if and only if x_k appears in the differential equation of x_j .*

Definition 2 (Causal consistency). *An estimator $\mathbf{f}_\theta = (f_1, \dots, f_d)$ is causally consistent if for any $\delta > 0$, there exists N_δ and T_δ such that for $n > N_\delta$ and $T > T_\delta$, we have $\|\partial_k f_j\|_{L_2} \neq 0^3$, for all $k, j \in \{1, \dots, d\}$ such that x_k is causally significant for x_j , and have $\|\partial_k f_j\|_{L_2} = 0$ otherwise, with probability at least $1 - \delta$.*

3.1 Graphical presentation

The structure of equations in (4) and the endogenous processes that appear in them can be represented by the associated directed graph $\mathcal{G} = (\mathbf{V}, \mathbf{E})$, where each endogenous process is associated with a distinct vertex in \mathbf{V} and there is a directed edge $(x_k \rightarrow x_j) \in \mathbf{E}$ if and only if process $x_k \in \mathbf{V}$ appears in the differential equation of $x_j \in \mathbf{V}$. Graphs associated with (4) are directed but not necessarily acyclic.

In the context of analytic vector fields \mathbf{f} , graphs G may be defined by the sparsity pattern of \mathbf{f} : $(x_k \rightarrow x_j) \in \mathbf{E}$ if and only if $\|\partial_k f_j\|_{L_2} \neq 0$ (which leads to our definition of causal consistency). We will refer to $G \in \{0, 1\}^{d \times d}$ as the associated adjacency matrix of the underlying graph \mathcal{G} . Graphs as defined above are a special case of Markov ordering graphs introduced by Simon [76] and of local independence graphs (involving (in)dependence relations between \mathbf{x} and $d\mathbf{x}$ in data), see e.g. [23, 22]. As a contrast with causal discovery in static data, for causally sufficient systems, there is a unique correspondence between local independencies in data and the underlying graph \mathcal{G} , see e.g. Proposition 3.6 by Mogensen et al. [50]. In other words, if local independencies can be estimated consistently, the associated causal graph can be recovered consistently.

3.2 Identifiability

Even if causal associations are identifiable in theory, in practice, with finite samples and complex functions, the map between model and data is not necessarily identifiable. Write $\mathcal{R}_n(\mathbf{f}_\theta) = \frac{1}{n} \sum_{i=1}^n \|\mathbf{y}_i - \hat{\mathbf{x}}(t_i)\|_2^2$ (the dependence on \mathbf{f}_θ is implicit in $\hat{\mathbf{x}}$) and $\mathcal{R}(\mathbf{f}_\theta)$ for its population counterpart. The difficulty arises from the geometry of the loss function around the set of loss minimizers,

$$\Theta^* = \{\theta \in \Theta : \mathcal{R}(\mathbf{f}_\theta) = \mathcal{R}(\mathbf{f}_{\theta_0})\}, \quad (7)$$

where Θ is the parameter space. The set Θ^* (of all weight vectors that produce the same input-output map as the generating model) can be quite complex and the behavior of a generic estimator in this set not necessarily reflect causal associations.

It is possible, however, to constrain the solution space to a subset of "well-behaved" optima for which G is uniquely identifiable even if the full set of parameters θ is not. It is sufficient for causality to identify the group structure of input layer parameters $[A_1^j]$ exactly, entire columns $[A_1^j]_{\cdot k}$ for $k = 1, \dots, d$ simultaneously set to zero or not to disentangle causal and spurious process associations. If this can be recovered exactly, then the inferred G corresponds to the

²From a physical perspective, on its own system (4) is purely symmetric, but once placed in the context of boundary conditions, because of entropic considerations, it defines unambiguous asymmetric relationships between processes that define causality.

³ $\partial_k f_j$ denotes the partial derivative with respect the k -th argument of f_j , $\|\cdot\|_{L_2}$ is the functional L_2 norm.

causal structure. Optimization with this group structure desiderata has been often considered before as a penalized optimization problem,

$$\arg \min_{\mathbf{f}_\theta} \mathcal{R}_n(\mathbf{f}_\theta), \quad \text{subject to} \quad d\mathbf{x}(t) = \mathbf{f}_\theta(\mathbf{x}(t))dt \quad \text{and} \quad \rho(\mathbf{f}_\theta) \leq \eta, \quad (8)$$

where we have suppressed the dependence of ρ on the sample size and time horizon for readability. Two popular constraints are the group lasso (GL) and the adaptive group lasso (AGL), see e.g. [91, 90], defined as,

$$\rho_{\text{GL}}(\mathbf{f}_\theta) := \lambda_{\text{GL}} \sum_{k,j=1}^d \|[A_1^j]_{\cdot k}\|_2, \quad \rho_{\text{AGL}}(\mathbf{f}_\theta) := \lambda_{\text{AGL}} \sum_{k,j=1}^d \frac{1}{\|[\hat{A}_1^j]_{\cdot k}\|_2^\gamma} \|[A_1^j]_{\cdot k}\|_2,$$

respectively, where \hat{A}_1^j is the GL estimate to problem (8), $\lambda_{\text{GL}}, \lambda_{\text{AGL}}$ determine the regularization strength and may vary with n and T , $\gamma > 0$ and $\|\cdot\|_2$ is the Euclidian norm. As with other adaptive lasso estimators, AGL uses its base estimator to provide a rough data-dependent estimate to shrink groups of parameters with different regularization strengths. As n and T grow, the weights for non-significant features get inflated while the weights for significant ones remain bounded, allowing AGL to exactly identify significant parameters.

The following generalization bound will be useful to define convergence rates for penalized solutions.

Lemma 1 (Generalization bound). *Assume Σ_n to be invertible and let $\alpha = (\alpha_1, \dots, \alpha_n)$ such that $\alpha_1 > \dots > \alpha_n > 0$ are its eigenvalues. For any $\delta > 0$, there exists $C_\delta > 0$ such that,*

$$|\mathcal{R}_n(f_\theta) - \mathcal{R}(f_\theta)| \leq C_\delta \left(\frac{\|\alpha\|_2}{n} \right) \sqrt{\log \left(\frac{n}{\|\alpha\|_2} \right)}, \quad (9)$$

with probability at least $1 - \delta$.

Proof. All proofs are given in the Appendix.

Remark on interpretation. Note that $\|\alpha\|_2 \leq \|\alpha\|_1 = n$ (since the data is assumed to be scaled to have variance 1 for all observations) and that larger values of $\|\alpha\|_2$ occur with a greater difference in magnitude in the entries of α . The difference in magnitude in the principal components of \mathbf{Y} is defined by the dependence between samples. A strong dependence between samples (as would be expected with frequently observed time series) leads to proportionally larger magnitude of α_1 (the first component of α) as more variance in the data is explained by a single direction of variation and thus decreases the effective sample size – making $\|\alpha\|_2$ closer to n . The bound formalizes the trade-off between the number of samples and their dependence. By increasing the observation frequency one can produce an arbitrarily large number of distinct samples but samples become more dependent and therefore less useful for concentration of the empirical error around its population value (unless one simultaneously increases the time horizon T).

We now show convergence and causal consistency of the adaptive group lasso penalized estimator. The following lemmas use a similar proof technique to Dinh et al. [20] with the difference that the convergence speeds differ due to sample dependency.

Lemma 2 (Convergence of Adaptive Group Lasso). *Let $\tilde{\theta}_n \in \Theta$ be the parameter solution of (8) with adaptive group lasso constraint. For any $\delta > 0$, assuming that $\lambda_{\text{AGL}} \rightarrow 0$ there exists $v > 0, C_\delta > 0, N_\delta > 0$ and $T_\delta > 0$ such that,*

$$\min_{\theta \in \Theta^*} \|\tilde{\theta}_n - \theta\| \leq C_\delta \left(\lambda_{\text{AGL}} + \left(\frac{\|\alpha\|_2}{n} \right) \sqrt{\log \left(\frac{n}{\|\alpha\|_2} \right)} \right)^{\frac{1}{v}} \quad (10)$$

with probability at least $1 - \delta$.

Lemma 3 (Causal consistency of Adaptive Group Lasso). *Let $\gamma > 0, \epsilon > 0, \nu > 0, \lambda_{\text{AGL}} = \Omega\left(\left(\frac{n}{\|\alpha\|_2}\right)^{-\gamma/\nu+\epsilon}\right)$, and $\lambda_{\text{AGL}} = \Omega(\lambda_{\text{GL}}^{\gamma+\epsilon})$, then the adaptive group lasso (solution to problem (8)) is causally consistent.*

Remark on interpretation. Lemma 3 implies that with increasing sample size and time horizon the graph G defined such that $[G]_{jk} = 0$ if and only if $\|[\hat{A}_1^j]_{\cdot k}\|_2 = 0$ is the causal graph with high probability. The group lasso will generally not be causally consistent because it forces all parameters to be equally penalized. Some evidence for this claim in the context of feature selection was provided by Hui Zou [91].

3.3 Algorithm: Neural Mechanistic Causality model

Neural ODEs proposed by Chen et al. [10] are a family of continuous-time models which define the hidden representation of a learning problem explicitly to be the solution to an ODE initial-value problem in which \mathbf{f}_θ is a free parameter

specified by a neural network. For each estimate of \mathbf{f}_θ , the forward trajectory can be computed using any numerical ODE solver:

$$\hat{\mathbf{x}}(t_1), \dots, \hat{\mathbf{x}}(t_n) = \text{ODESolve}(\mathbf{f}_\theta, \mathbf{x}(t_0), t_1, \dots, t_n), \quad (11)$$

and thus implicitly enforcing the constraint $d\mathbf{x}(t) = \mathbf{f}_\theta(\mathbf{x}(t))dt$ while optimizing for $\mathcal{R}_n(\mathbf{f}_\theta)$ and thus solving for (3). Gradients with respect to θ may be computed with adjoint sensitivities and a gradient descent algorithm can be used to backpropagate through the ODE solver and the continuous state dynamics to update the parameters of \mathbf{f}_θ , as shown by Chen et al. [10].

Remark on estimated graph. With the construction presented in (5), constraining the k -th column of each A_1^j to be zero in euclidian norm effectively forces $\|\partial_k f_j\|_{L_2} = 0$ and vice versa. We may thus recover the dependency graph \mathcal{G} by inspecting the values estimated for the norm of column vectors $\|[A_1^j]_{\cdot k}\|_2$ for each j and k in $\{1, \dots, d\}$. In experiments, we use a weighted version of the adjacency matrix of $\mathcal{G} - G$ defined such that $[G]_{jk} := \|[A_1^j]_{\cdot k}\|_2$.

Remark on optimization. The adaptive group lasso constraint is not differentiable and non-separable which precludes applying coordinate optimization algorithms. However, a wide variety of techniques from optimization theory have been developed to tackle this case. A general way of doing so is through proximal optimization, see e.g. [55, 58] that leads to exact zeros in the columns of the input matrices without having to use a cut-off value for selection. The proximal step for the group lasso penalty is given by a group soft-thresholding operation on the input weights and can be interleaved with conventional gradient update steps. Please find all details in the Appendix.

We call this algorithm for causal discovery the Neural Mechanistic Causality (NMC) model.

4 Experiments

This section makes performance comparisons on controlled experiments designed to analyzed 4 important challenges for causal discovery with time series data: the **irregularity** of observation times, the **sparsity** of observation times, the **non-linearity** of dynamics, and the **differing scale** of processes in a system.

We benchmark NMC against a variety of algorithms, namely:

- Three representative vector autoregression models: Neural Granger causality [80] in two instantiations, one based on feed forward neural networks (**NGC-MLP**) and one based on recurrent neural networks (**NGC-LSTM**), and the Structural Vector Autoregression Model (**SVAM**) [35] (an extension of the LiNGAM algorithm to time series).
- A representative independence-based approach to causal discovery with time series data: **PCMCI** [68], extending the PC algorithm.
- A representative two-stage collocation method we call Dynamic Causal Modelling (**DCM**) in which derivatives are first estimated on interpolations of the data and a penalized neural network is learned to infer G (extending the linear models of [64, 86, 8]).

Metric. We seek to recover the adjacency matrix of causal associations G between the state of all variables and their variation. All experiments are repeated 100 times and we report mean and standard deviations of the false discovery rate (FDR) and true positive rate (TPR) in recovery performance of G . Thresholds for determining the presence and absence of edges in G were chosen for maximum F_1 score. For applications in biology, false positives and false negatives can have very different failure interpretations; we choose to report both TPR and FDR explicitly to emphasize the trade-offs of each method when used in practice. Comparisons based on the area under the ROC curve (evaluating the whole range of possible thresholds) are given in the Appendix. Experiments comparing different regularization schemes as well as precise experimental details regarding neural network architectures and implementation software may also be found in the Appendix.

4.1 Lorenz’s chaotic model

We begin by considering **irregularly** sampled data and **sparsely** sampled data to investigate the benefit of modelling dynamics continuously in time.

We use Lorenz’s model [46] as an example of the kind of chaotic systems observed in biology e.g., electrodynamics of cardiac tissue [30], gene regulatory networks [34], etc. The continuous dynamics in a d -dimensional Lorenz model are,

$$\frac{d}{dt}x_i(t) = (x_{i+1}(t) - x_{i-2}(t)) \cdot x_{i-1}(t) - x_i(t) + F,$$

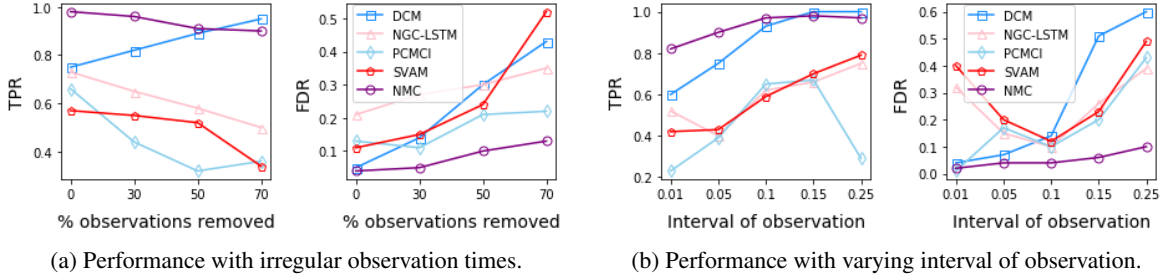


Figure 2: True positive (higher better) and false discovery (lower better) performance comparisons on Lorenz’s model. Thresholds are chosen for maximum F_1 score. We omitted plotting NGC-MLP which gave very similar results to NGC-LSTM.

for $i = 1, \dots, d$, where $x_{-1}(t) := x_{d-1}(t)$, $x_0(t) := x_p(t)$, $x_{d+1}(t) := x_1(t)$ and F is a forcing constant which determines the level of non-linearity and chaos in the series. The initial state of each variable is sampled from a standard Gaussian distribution, d is set to 10 and F to 10. We illustrate sample trajectories of this system in Figure 1.

- Irregularly sampled data is generated by removing randomly a percentage of the regularly sampled data (with a 0.1 time interval between observations and 1000 observations). For consistency of causality, discrete-time methods here use cubic spline interpolations evaluated at regular time intervals.
- Frequently and sparsely sampled data is generated by varying the time interval of observation (the data always being regularly sampled).

Results. Performance results are given in Figure 2. It is important here to look at both TPR and FDR panels for each experiment. For instance, a model returning always a fully connected graph G will have $\text{TPR} = 1$ but $\text{FDR} = 0$. Thus looking at both measures together, NMC significantly improves performance over competing approaches. And moreover, NMC’s performance is more robust (worsens less) with increasingly irregular sampling and with increasingly sparse data. The behaviour of discrete-time methods is highly heterogeneous. NGC-LSTM, SVAM and PCMCI are highly dependent on the interval of observation, both too frequent and too sparse measurement times leading to poor FDR. Similarly, as we introduce more irregular sampling TPR decreases and FDR increases which we hypothesize is due to error introduced in the interpolation. This pattern is consistent with our intuition (illustrated in Figure 1) that direct and indirect effects become indistinguishable in discrete time and thus have high FDR with irregular or sparse data. In the case of DCM, it has good performance with frequently observed time series and regular data but rapidly deteriorates otherwise which we hypothesize is due to worsening approximations of derivatives in those cases.

4.2 Rössler’s hyperchaotic model

Next, we consider data with **non-linear** dynamics, said to exhibit *hyperchaotic* behaviour, to demonstrate the flexibility of learned functional relationships.

Chaotic systems, such as Lorenz’s model, are characterized by one direction of exponential spreading. If the number of directions of spreading is greater than one the behavior of the system is hyperchaotic (see e.g. [4]), and much more complicated to predict. In practice this has been observed in chemical reactions [24] and EEG models of the brain [14]. Rössler proposed in 1979 [65] the first hyperchaotic system of differential equations and here we consider a generalization of this model to arbitrary dimensions and non-linear vector fields as in [49]. The d -dimensional generalized Rössler model is given by,

$$\begin{aligned} \frac{d}{dt}x_1(t) &= ax_1(t) - x_2(t), \\ \frac{d}{dt}x_i(t) &= \sin(x_{i-1}(t)) - \sin(x_{i+2}(t)), \quad i = 2, \dots, d-1, \\ \frac{d}{dt}x_d(t) &= \epsilon + bx_d(t) \cdot (x_{d-1}(t) - q). \end{aligned}$$

We use typical parameters for hyperchaotic behaviour: $a = 0$, $\epsilon = 0.1$, $b = 4$, $q = 2$, as in [49]. This system is observed over a sequence of 1000 time points with a 0.1 time unit interval after randomly initializing each variable to a sample from a standard Gaussian distribution and d is set to 10 and 50 to evaluate also performance in higher dimensions.

	Rössler ($d = 10$)		Rössler ($d = 50$)		Glycolysis	
	TPR \uparrow	FDR \downarrow	TPR \uparrow	FDR \downarrow	TPR \uparrow	FDR \downarrow
NGC-MLP	.45 (.05)	.55 (.06)	.31 (.04)	.67 (.06)	.60 (.04)	.51 (.05)
NGC-LSTM	.49 (.04)	.53 (.04)	.38 (.04)	.64 (.08)	.69 (.04)	.40 (.04)
SVAM	.17 (.03)	.84 (.04)	.03 (.08)	.95 (.09)	.61 (.02)	.53 (.07)
PCMRI	.10 (.03)	.92 (.02)	.09 (.06)	.89 (.06)	.56 (.05)	.43 (.06)
DCM	.87 (.01)	.10 (.04)	.97 (.01)	.31 (.07)	.67 (.04)	.49 (.05)
NMC	.96 (.01)	.02 (.01)	.95 (.01)	.04 (.01)	.84 (.04)	.44 (.09)

Table 1: Performance comparisons on Rössler’s model and the yeast Glycolysis model.

Results. Performance results are given in Table 1 and the contrast between non-linear and linear methods is stark. NMC continues to strongly outperform other methods with almost perfect recovery of the graph G in both low and high-dimensional regimes. The strongest baseline is DCM which also models causality in continuous-time.

4.3 Model of oscillations in yeast glycolysis

We conclude with an experiment from the pharmacology literature which makes extensive use of dynamical models to determine the interaction patterns of drugs in the body. In these systems, it is the **difference in scale** of different biochemicals that makes causal discovery difficult.

The glycolytic oscillator model is a standard benchmark for this kind of systems. It simulates the cycles of the metabolic pathway that breaks down glucose in cells. We simulate the system presented in equation (19) by Daniels et al. [15] defined by 7 biochemical components and fully described in the Appendix.

For biology in particular, a feature of NMC is that it explicitly discovers f and its causal features such that the model can be used to simulate the system and the effect of interventions by modifying the weights of a trained network which may have a large impact on the design of (laboratory) experiments. We show, for illustration, NMC’s simulation of the glycolytic oscillator in Figure 3, which successfully recovers the true dynamics.

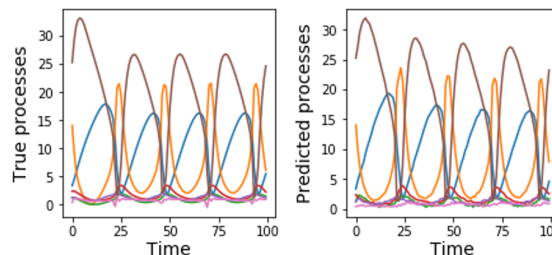


Figure 3: True and NMC-estimated Glycolytic oscillations.

Results. Table 1 shows that performance on this data is more heterogeneous. Although NMC outperforms or is competitive with other methods, FDR is high. Better understanding how to model causality in systems with different scales (see this explicitly in Figure 3 with numerous variables with values equal to a small fraction of the largest observations) thus remains an important challenge.

5 Discussion

An emerging trend in biology, climate science and healthcare is the measurement of increasing amounts of datatypes (individual gene transcript levels, protein abundances, molecular concentrations of pollution in the air, biomarkers in the hospital, etc.) on an increasing resolution but with heterogeneous observation patterns. A causal model that is stable over a large number of variables, over a large number of sampling frequencies and observation patterns has attractive properties to scientists in all these domains. In this paper, we have discussed causal discovery from a mechanistic perspective in dynamical systems and have shown the consistency of penalized least squares problems in general models of ODEs with analytic vector fields. Our contribution is also a novel causal discovery algorithm, Neural Mechanistic Causality, that models the latent vector field explicitly with penalized extensions to Neural ODEs and is applicable to general irregularly-sampled multivariate time series. We conclude with some additional remarks.

- **Causal sufficiency.** In general, we cannot expect to recover causal interactions if unobserved processes influence the dynamics of the system. Anecdotally however, a form of violation of this assumption was included in the Lorenz system (perturbed by a factor F which is not modelled) for which we achieve almost perfect causal recovery. Some

robustness to violations of this condition may thus be expected although we did not perform a formal investigation of this phenomenon.

- **Stochastic differential equations.** The data criterion $\frac{1}{n} \sum_{i=1}^n \|\mathbf{y}_i - \hat{\mathbf{x}}(t_i)\|_2^2$ may be equally interpreted as the log-likelihood for observations from the stochastic differential equation:

$$d\mathbf{y}(t) = \mathbf{f}(\mathbf{y}(t))dt + dW(t), \quad (12)$$

where $W(t)$ is a d -dimensional Brownian motion. NMC may be thought of as profiling an estimate of the realized Brownian motion. Convergence and consistency results under this model hold with the difference that variances (diagonal elements $\sigma_i^2, i = 1, \dots, n$ of Σ_n) are heteroscedastic (driven by the Brownian motion) which in practice means that the norm of eigenvalues $\|(\alpha_1, \dots, \alpha_n)\|_2$ is replaced with $\|(\alpha_1/\sigma_1, \dots, \alpha_n/\sigma_n)\|_2$.

- **Switching dynamical systems.** In the context of a Neural ODE, \mathbf{f} was defined using a continuous neural network and $\mathbf{x}(t)$ is always continuous in t . Trajectories modeled by an ODE can thus have limited representation capabilities when discontinuities in the state occur. Examples are switching dynamical systems which are hybrid discrete and continuous systems that choose which dynamics to follow based on a discrete switch, and are popular in neuroscience and finance (see e.g. [26]).

For these systems, a practical extension would be to follow [9] and modify the gradient update to include discrete changes in the event state in which case, to infer the causal graph, partial derivatives $\partial_k f_j$ would be defined piece-wise.

Acknowledgements

We thank Jeremy England and Hagen Triendl for helpful feedback. This work was supported by the Alan Turing Institute under the EPSRC grant EP/N510129/1, the ONR and the NSF grants number 1462245 and number 1533983.

References

- [1] Odd O Aalen, Kjetil Røysland, Jon Michael Gran, and Bruno Ledergerber. Causality, mediation and time: a dynamic viewpoint. *Journal of the Royal Statistical Society: Series A (Statistics in Society)*, 175(4):831–861, 2012.
- [2] Odd Olai Aalen, Kjetil Røysland, Jon Michael Gran, Roger Kouyos, and Tanja Lange. Can we believe the dags? a comment on the relationship between causal dags and mechanisms. *Statistical methods in medical research*, 25(5):2294–2314, 2016.
- [3] Robert Adamek, Stephan Smeekes, and Ines Wilms. Lasso inference for high-dimensional time series. *arXiv preprint arXiv:2007.10952*, 2020.
- [4] Roberto Barrio, M Angeles Martínez, Sergio Serrano, and Daniel Wilczak. When chaos meets hyperchaos: 4d rössler model. *Physics Letters A*, 379(38):2300–2305, 2015.
- [5] José Bento, Morteza Ibrahimi, and Andrea Montanari. Learning networks of stochastic differential equations. *arXiv preprint arXiv:1011.0415*, 2010.
- [6] Tineke Blom and Joris M Mooij. Generalized structural causal models. *arXiv preprint arXiv:1805.06539*, 2018.
- [7] Annalisa Bracco, Fabrizio Falasca, Athanasios Nenes, Ilias Fountalis, and Constantine Dovrolis. Advancing climate science with knowledge-discovery through data mining. *npj Climate and Atmospheric Science*, 1(1):1–6, 2018.
- [8] Steven L Brunton, Joshua L Proctor, and J Nathan Kutz. Discovering governing equations from data by sparse identification of nonlinear dynamical systems. *Proceedings of the national academy of sciences*, 113(15):3932–3937, 2016.
- [9] Ricky TQ Chen, Brandon Amos, and Maximilian Nickel. Learning neural event functions for ordinary differential equations. *arXiv preprint arXiv:2011.03902*, 2020.
- [10] Ricky TQ Chen, Yulia Rubanova, Jesse Bettencourt, and David K Duvenaud. Neural ordinary differential equations. In *Advances in neural information processing systems*, pages 6571–6583, 2018.
- [11] Shizhe Chen, Ali Shojaie, and Daniela M Witten. Network reconstruction from high-dimensional ordinary differential equations. *Journal of the American Statistical Association*, 112(520):1697–1707, 2017.
- [12] Yonghong Chen, Govindan Rangarajan, Jianfeng Feng, and Mingzhou Ding. Analyzing multiple nonlinear time series with extended granger causality. *Physics Letters A*, 324(1):26–35, 2004.
- [13] Victor Chernozhukov, Wolfgang K Härdle, Chen Huang, and Weining Wang. Lasso-driven inference in time and space. *Available at SSRN 3188362*, 2019.
- [14] Mathew P Dafilis, Federico Frascoli, Peter J Cadusch, and David TJ Liley. Four dimensional chaos and intermittency in a mesoscopic model of the electroencephalogram. *Chaos: An Interdisciplinary Journal of Nonlinear Science*, 23(2):023111, 2013.
- [15] Bryan C Daniels and Ilya Nemenman. Efficient inference of parsimonious phenomenological models of cellular dynamics using s-systems and alternating regression. *PloS one*, 10(3):e0119821, 2015.
- [16] David Danks and Sergey Plis. Learning causal structure from undersampled time series. 2013.
- [17] Denver Dash. Restructuring dynamic causal systems in equilibrium. In *AISTATS*. Citeseer, 2005.
- [18] Itai Dattner, Chris AJ Klaassen, et al. Optimal rate of direct estimators in systems of ordinary differential equations linear in functions of the parameters. *Electronic Journal of Statistics*, 9(2):1939–1973, 2015.
- [19] Vanessa Didelez. Asymmetric separation for local independence graphs. *arXiv preprint arXiv:1206.6841*, 2012.
- [20] Vu Dinh and Lam Si Tung Ho. Consistent feature selection for analytic deep neural networks. *arXiv preprint arXiv:2010.08097*, 2020.
- [21] Phil Dowe. Wesley salmon’s process theory of causality and the conserved quantity theory. *Philosophy of science*, 59(2):195–216, 1992.
- [22] Michael Eichler. Causal inference with multiple time series: principles and problems. *Philosophical Transactions of the Royal Society A: Mathematical, Physical and Engineering Sciences*, 371(1997):20110613, 2013.
- [23] Michael Eichler and Vanessa Didelez. Causal reasoning in graphical time series models. *arXiv preprint arXiv:1206.5246*, 2012.
- [24] M Eiswirth, Th-M Kruehl, G Ertl, and FW Schneider. Hyperchaos in a chemical reaction. *Chemical physics letters*, 193(4):305–310, 1992.

- [25] Jerome Friedman, Trevor Hastie, and Robert Tibshirani. Sparse inverse covariance estimation with the graphical lasso. *Biostatistics*, 9(3):432–441, 2008.
- [26] Karl Friston. Causal modelling and brain connectivity in functional magnetic resonance imaging. *PLoS Biol*, 7(2):e1000033, 2009.
- [27] Karl J Friston, Lee Harrison, and Will Penny. Dynamic causal modelling. *Neuroimage*, 19(4):1273–1302, 2003.
- [28] Stuart Glennan. Rethinking mechanistic explanation. *Philosophy of science*, 69(S3):S342–S353, 2002.
- [29] Stuart Glennan. Mechanisms, causes, and the layered model of the world. *Philosophy and Phenomenological Research*, 81(2):362–381, 2010.
- [30] Ary L Goldberger and Bruce J West. Applications of nonlinear dynamics to clinical cardiology. *Annals of the New York Academy of Sciences*, 504:195–213, 1987.
- [31] Mingming Gong, Kun Zhang, Bernhard Schoelkopf, Dacheng Tao, and Philipp Geiger. Discovering temporal causal relations from subsampled data. In *International Conference on Machine Learning*, pages 1898–1906. PMLR, 2015.
- [32] Clive WJ Granger. Investigating causal relations by econometric models and cross-spectral methods. *Econometrica: journal of the Econometric Society*, pages 424–438, 1969.
- [33] Markus Heinonen, Cagatay Yildiz, Henrik Mannerström, Jukka Intosalmi, and Harri Lähdesmäki. Learning unknown ode models with gaussian processes. In *International Conference on Machine Learning*, pages 1959–1968. PMLR, 2018.
- [34] Mathias L Heltberg, Sandeep Krishna, and Mogens H Jensen. On chaotic dynamics in transcription factors and the associated effects in differential gene regulation. *Nature communications*, 10(1):1–10, 2019.
- [35] Aapo Hyvärinen, Kun Zhang, Shohei Shimizu, and Patrik O Hoyer. Estimation of a structural vector autoregression model using non-gaussianity. *Journal of Machine Learning Research*, 11(5), 2010.
- [36] Rolf Isermann and Marco Münchhof. *Identification of dynamic systems: an introduction with applications*. Springer Science & Business Media, 2010.
- [37] Yumi Iwasaki and Herbert A Simon. Causality and model abstraction. *Artificial intelligence*, 67(1):143–194, 1994.
- [38] Saurabh Khanna and Vincent YF Tan. Economy statistical recurrent units for inferring nonlinear granger causality. *arXiv preprint arXiv:1911.09879*, 2019.
- [39] Anders Bredahl Kock and Laurent Callot. Oracle inequalities for high dimensional vector autoregressions. *Journal of Econometrics*, 186(2):325–344, 2015.
- [40] Petter Kristensen and Odd O Aalen. Understanding mechanisms: opening the "black box" in observational studies. *Scandinavian journal of work, environment & health*, 39(2):121–124, 2013.
- [41] Rebecca M Kuiper and Oisín Ryan. Drawing conclusions from cross-lagged relationships: Re-considering the role of the time-interval. *Structural Equation Modeling: A Multidisciplinary Journal*, 25(5):809–823, 2018.
- [42] Ismael Lemhadri, Feng Ruan, and Rob Tibshirani. LassoNet: Neural networks with feature sparsity. In *International Conference on Artificial Intelligence and Statistics*, pages 10–18. PMLR, 2021.
- [43] David Lewis. Counterfactual dependence and time’s arrow. *Noûs*, pages 455–476, 1979.
- [44] David K Lewis. *Void and object*. Department of Philosophy, University of Melbourne, 1998.
- [45] Yifeng Li, Chih-Yu Chen, and Wyeth W Wasserman. Deep feature selection: theory and application to identify enhancers and promoters. *Journal of Computational Biology*, 23(5):322–336, 2016.
- [46] Edward N Lorenz. Predictability: A problem partly solved. In *Proc. Seminar on predictability*, volume 1, 1996.
- [47] Peter Machamer. Activities and causation: The metaphysics and epistemology of mechanisms. *International studies in the philosophy of science*, 18(1):27–39, 2004.
- [48] Ričards Marcinkevičs and Julia E Vogt. Interpretable models for granger causality using self-explaining neural networks. *arXiv preprint arXiv:2101.07600*, 2021.
- [49] Th Meyer, MJ Bünner, A Kittel, and J Parisi. Hyperchaos in the generalized rössler system. *Physical Review E*, 56(5):5069, 1997.
- [50] Søren Wengel Mogensen, Niels Richard Hansen, et al. Markov equivalence of marginalized local independence graphs. *The Annals of Statistics*, 48(1):539–559, 2020.

- [51] Søren Wengel Mogensen, Daniel Malinsky, and Niels Richard Hansen. Causal learning for partially observed stochastic dynamical systems. In *UAI*, pages 350–360, 2018.
- [52] Joris M Mooij, Dominik Janzing, and Bernhard Schölkopf. From ordinary differential equations to structural causal models: the deterministic case. *arXiv preprint arXiv:1304.7920*, 2013.
- [53] Yuval Nardi and Alessandro Rinaldo. Autoregressive process modeling via the lasso procedure. *Journal of Multivariate Analysis*, 102(3):528–549, 2011.
- [54] Roxana Pamfil, Nisara Sriwattanaworachai, Shaan Desai, Philip Pilgerstorfer, Konstantinos Georgatzis, Paul Beaumont, and Bryon Aragam. Dynotears: Structure learning from time-series data. In *International Conference on Artificial Intelligence and Statistics*, pages 1595–1605. PMLR, 2020.
- [55] Neal Parikh and Stephen Boyd. Proximal algorithms. *Foundations and Trends in optimization*, 1(3):127–239, 2014.
- [56] Judea Pearl. *Causality*. Cambridge university press, 2009.
- [57] Jonas Peters, Stefan Bauer, and Niklas Pfister. Causal models for dynamical systems. *arXiv preprint arXiv:2001.06208*, 2020.
- [58] Nicholas G Polson, James G Scott, Brandon T Willard, et al. Proximal algorithms in statistics and machine learning. *Statistical Science*, 30(4):559–581, 2015.
- [59] Huw Price. Agency and probabilistic causality. *The British Journal for the Philosophy of Science*, 42(2):157–176, 1991.
- [60] Xiaojie Qiu, Qi Mao, Ying Tang, Li Wang, Raghav Chawla, Hannah A Pliner, and Cole Trapnell. Reversed graph embedding resolves complex single-cell trajectories. *Nature methods*, 14(10):979, 2017.
- [61] Federica Raia. Causality in complex dynamic systems: A challenge in earth systems science education. *Journal of Geoscience Education*, 56(1):81–94, 2008.
- [62] Maziar Raissi. Deep hidden physics models: Deep learning of nonlinear partial differential equations. *The Journal of Machine Learning Research*, 19(1):932–955, 2018.
- [63] Maziar Raissi, Paris Perdikaris, and George Em Karniadakis. Physics informed deep learning (part i): Data-driven solutions of nonlinear partial differential equations. *arXiv preprint arXiv:1711.10561*, 2017.
- [64] Jim O Ramsay, Giles Hooker, David Campbell, and Jiguo Cao. Parameter estimation for differential equations: a generalized smoothing approach. *Journal of the Royal Statistical Society: Series B (Statistical Methodology)*, 69(5):741–796, 2007.
- [65] OE Rossler. An equation for hyperchaos. *Physics Letters A*, 71(2-3):155–157, 1979.
- [66] Paul K Rubenstein, Stephan Bongers, Bernhard Schölkopf, and Joris M Mooij. From deterministic odes to dynamic structural causal models. *arXiv preprint arXiv:1608.08028*, 2016.
- [67] Donald B Rubin. Causal inference using potential outcomes: Design, modeling, decisions. *Journal of the American Statistical Association*, 100(469):322–331, 2005.
- [68] J Runge, D Sejdinovic, and S Flaxman. Detecting causal associations in large nonlinear time series datasets. *arXiv preprint arXiv:1702.07007*, 2017.
- [69] Jakob Runge. Causal network reconstruction from time series: From theoretical assumptions to practical estimation. *Chaos: An Interdisciplinary Journal of Nonlinear Science*, 28(7):075310, 2018.
- [70] Jakob Runge, Sebastian Bathiany, Erik Bollt, Gustau Camps-Valls, Dim Coumou, Ethan Deyle, Clark Glymour, Marlene Kretschmer, Miguel D Mahecha, Jordi Muñoz-Marí, et al. Inferring causation from time series in earth system sciences. *Nature communications*, 10(1):1–13, 2019.
- [71] Wesley C Salmon. *Scientific explanation and the causal structure of the world*. Princeton University Press, 1984.
- [72] Francisco Sanchez-Vega, Marco Mina, Joshua Armenia, Walid K Chatila, Augustin Luna, Konnor C La, Sofia Dimitriadoy, David L Liu, Havish S Kantheti, Sadegh Saghafinia, et al. Oncogenic signaling pathways in the cancer genome atlas. *Cell*, 173(2):321–337, 2018.
- [73] Thomas Schreiber. Measuring information transfer. *Physical review letters*, 85(2):461, 2000.
- [74] Peter Schulam and Suchi Saria. Reliable decision support using counterfactual models. In *Advances in Neural Information Processing Systems*, pages 1697–1708, 2017.
- [75] Shai Shalev-Shwartz and Shai Ben-David. *Understanding machine learning: From theory to algorithms*. Cambridge university press, 2014.

- [76] Herbert A Simon. On the definition of the causal relation. *The Journal of Philosophy*, 49(16):517–528, 1952.
- [77] Christopher A Sims. Macroeconomics and reality. *Econometrica: journal of the Econometric Society*, pages 1–48, 1980.
- [78] Hossein Soleimani, Adarsh Subbaswamy, and Suchi Saria. Treatment-response models for counterfactual reasoning with continuous-time, continuous-valued interventions. *arXiv preprint arXiv:1704.02038*, 2017.
- [79] Peter Spirtes, Clark N Glymour, Richard Scheines, and David Heckerman. *Causation, prediction, and search*. MIT press, 2000.
- [80] Alex Tank, Ian Covert, Nicholas Foti, Ali Shojaie, and Emily Fox. Neural granger causality for nonlinear time series. *arXiv preprint arXiv:1802.05842*, 2018.
- [81] Cole Trapnell, Davide Cacchiarelli, Jonna Grimsby, Prapti Pokharel, Shuqiang Li, Michael Morse, Niall J Lennon, Kenneth J Livak, Tarjei S Mikkelsen, and John L Rinn. The dynamics and regulators of cell fate decisions are revealed by pseudotemporal ordering of single cells. *Nature biotechnology*, 32(4):381, 2014.
- [82] James M Varah. A spline least squares method for numerical parameter estimation in differential equations. *SIAM Journal on Scientific and Statistical Computing*, 3(1):28–46, 1982.
- [83] Philippe Wenk, Gabriele Abbati, Michael A Osborne, Bernhard Schölkopf, Andreas Krause, and Stefan Bauer. Odin: Ode-informed regression for parameter and state inference in time-continuous dynamical systems. In *Proceedings of the AAAI Conference on Artificial Intelligence*, volume 34, pages 6364–6371, 2020.
- [84] Jon Williamson. Mechanistic theories of causality part i. *Philosophy Compass*, 6(6):421–432, 2011.
- [85] James Woodward. A theory of singular causal explanation. *Erkenntnis*, 21(3):231–262, 1984.
- [86] Hulin Wu, Tao Lu, Hongqi Xue, and Hua Liang. Sparse additive ordinary differential equations for dynamic gene regulatory network modeling. *Journal of the American Statistical Association*, 109(506):700–716, 2014.
- [87] Zuogon Yue, Johan Thunberg, and Jorge Goncalves. Inverse problems for matrix exponential in system identification: system aliasing. *arXiv preprint arXiv:1605.06973*, 2016.
- [88] Anru R Zhang and Yuchen Zhou. On the non-asymptotic and sharp lower tail bounds of random variables. *Stat*, 9(1):e314, 2020.
- [89] Huaqing Zhang, Jian Wang, Zhanquan Sun, Jacek M Zurada, and Nikhil R Pal. Feature selection for neural networks using group lasso regularization. *IEEE Transactions on Knowledge and Data Engineering*, 32(4):659–673, 2019.
- [90] Peng Zhao and Bin Yu. On model selection consistency of lasso. *Journal of Machine learning research*, 7(Nov):2541–2563, 2006.
- [91] Hui Zou. The adaptive lasso and its oracle properties. *Journal of the American statistical association*, 101(476):1418–1429, 2006.

Appendix

This appendix provides additional material accompanying the main body of the paper: "Consistency of mechanistic causal discovery in continuous-time using Neural ODEs".

It is outlined as follows:

- Section [A](#) discusses additional related work.
 - Section [A.1](#) contrasts discrete-time and continuous-time accounts of causality considering inconsistencies in causal discovery by modelling the underlying continuous-time process in discrete-time and the differences in graphical presentation.
 - Section [A.2](#) discusses other work modelling differential equations.
 - Section [A.3](#) briefly comments on the philosophical debate around the nature of causality and its ramifications in machine learning.
- Section [B](#) proves lemmas discussed in the main body of this paper.
- Section [C](#) includes all experimental details and an additional experiment.
 - Section [C.1](#) gives experiment results in terms of the area under the ROC curve.
 - Section [C.2](#) presents a purely synthetic data generating mechanism and tests different regularization schemes to justify the adaptive group lasso empirically.
 - Section [C.3](#) includes algorithm implementation details.
 - Section [C.4](#) gives the data generating system for the Glycolysis experiment.

A Related work

A.1 Discrete-time accounts of causality

A first practical definition of causality for inference with time series data was given by Granger [32]. A time series x_i is said to *Granger-cause* x_j if omitting the past of a time series x_i in a time series model including x_j 's own and other covariates' past increases the prediction error of the next time step of x_j . Implementations of this principle are variants of vector auto-regressive (VAR) models and its extensions (see e.g. [77, 12, 80, 54]), for example in the linear case assuming,

$$\mathbf{x}(t + \Delta t) = B_1 \mathbf{x}(t) + \dots + B_k \mathbf{x}(t - k\Delta t) + \epsilon(t), \quad \epsilon(t) \sim P, \quad (13)$$

for some distribution P . Each one of the matrices B_1, \dots, B_k then describe *lagged* causal relationships with different lags. Subsampling occurs when the frequency of observation is lower than Δt and renders VAR models generally unidentifiable although specific exceptions exist and have been explored in [31, 16]. Alternatives to VAR models include the PC algorithm with conditional independence testing methods accounting for auto-correlations between successive observations as done by Runge et al. [69, 68, 70] and transfer entropy principles [73].

The lagged nature of causal associations in VAR models is a fundamental contrast with a *mechanistic* understanding of causality in which causal claims are claims about the existence of a mechanism or process that mediates events at one time with events at a later time *continuously in time*. In other words, in a mechanistic interpretation of causality there can be no time gaps between a cause and its effect. It is important to mention however, that such an account may not fit *every* situation we would commonly associate with the presence of causal relationships but it is a useful description of systems evolving continuously in time and aligns well with the mathematics of differential equations that is already used to describe most dynamical systems.

A.1.1 Inconsistencies with causal discovery

In this section, we explain in more detail with an example why, from a learning perspective, causal discovery defined in discrete-time is fundamentally an ill-posed problem under the assumption that the physical process governing observations is a continuously evolving dynamical system.

Example. Assume the true dynamics of two processes $\mathbf{x}(t) = (x_1(t), x_2(t))^T$ to be given by,

$$\frac{d}{dt} \mathbf{x}(t) = A \mathbf{x}(t), \quad A = \begin{pmatrix} -1 & 2 \\ -4 & -0.5 \end{pmatrix}, \quad (14)$$

The underlying dynamics are given by A : x_2 causing an increase in the rate of change of x_1 (with value 2) while x_2 having a large negative causal effect on the rate of change of x_1 (with value -4). The corresponding discrete-time model (with one time lag for simplicity) may be defined as,

$$\mathbf{x}(t + \Delta t) = B_{\Delta t} \cdot \mathbf{x}(t), \quad (15)$$

where Δt is the time interval of observation. The two models are connected by a simple relation, given by $B_{\Delta t} = \exp\{A \cdot \Delta t\}$, that can be used to uniquely compute the off-diagonal entries $[B_{\Delta t}]_{12}$ and $[B_{\Delta t}]_{21}$ indicating the strength of "causal" effects $x_2 \rightarrow x_1$ and $x_1 \rightarrow x_2$ respectively, under the Granger-causality paradigm [32].

As a first observation, irrespective of the time interval Δt note that a single discrete-time model $B_{\Delta t}$ may describe multiple underlying mechanisms A as matrix logarithms $\log B_{\Delta t}$ are not identified if $B_{\Delta t}$ has complex eigenvalues (see e.g. [87] for a formal result). Second, for a single model defined by A the discrete-time causal interpretation (i.e. $B_{\Delta t}$) may change dramatically as a function of the time interval Δt at which the process is observed, as shown in Figure 4. Describing causality within dynamical systems in discrete-time is inherently an ill-posed problem. In fact, only for dynamical systems that are bivariate, stable, and non-oscillating can we expect consistent conclusions at all measurement intervals.

Proposition 1 (Causal inconsistency in discrete time [41]). *The sign of off-diagonal entries of $B_{\Delta t}$ and A agree for all time intervals $\Delta t > 0$ if A defines a bivariate, stable, and non-oscillating system of differential equations.*

Proof. Using the relationship $B_{\Delta t} = \exp\{A \cdot \Delta t\}$ we can write,

$$B_{\Delta t} = V^{-1} \exp\{D_{A \cdot \Delta t}\} V \quad (16)$$

where $D_{A \cdot \Delta t}$ represents the diagonal matrix containing the scalar exponentials of the eigenvalues of A multiplied by the scalar Δt and V is the matrix of eigenvectors. This can be used to relate two estimated discrete-time matrix coefficients with each other,

$$B_{\Delta_2 t} = B_{\Delta_1 t}^{(\Delta_2 t / \Delta_1 t)} \quad (17)$$

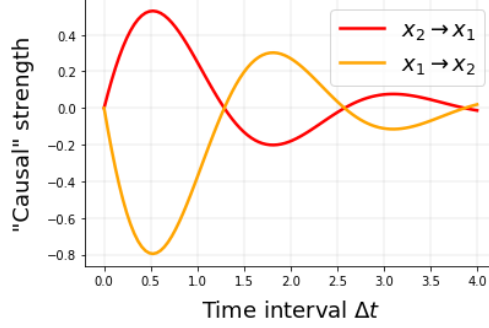


Figure 4: Strength and sign of the interaction as given by a discrete-time model as a function of the time interval the processes are observed.

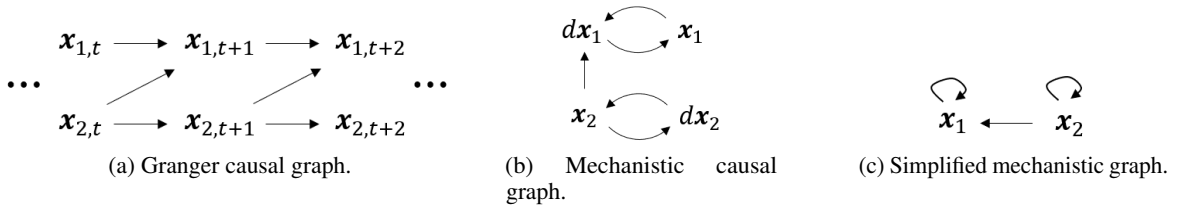


Figure 5: Graphical representations of Granger and mechanistic causality from systems (18) and (19).

Consider now a bivariate process with eigenvalues of an estimated $B_{\Delta_1 t}$ denoted by λ_1 and λ_2 , and let $\Delta_2 t = n \cdot \Delta_1 t$. Then, misleading causal conclusions are obtained if the sign of the entries of $B_{\Delta_2 t}$ differ from $B_{\Delta_1 t}$. In this case they may be computed explicitly. It holds that the sign of off-diagonal entries are equal if and only if $(\lambda_1 - \lambda_2)$ (determining the sign of entries of $B_{\Delta_1 t}$) and $(\lambda_1^n - \lambda_2^n)$ (determining the sign of entries of $B_{\Delta_2 t}$) are equal. This is the case if both λ_1 and λ_2 lie between 0 and 1 i.e., a stable, bi-variate, non-oscillating system, but will not hold in general otherwise.

Counter-examples of discrepancies can be found for many other types of differential equations in [41].

A.1.2 Differences in graphical representation

The graphical representation similarly differs between discrete-time and continuous-time accounts of causality. The defining feature of continuous accounts is that all causation is given by a derivative (e.g. dx) contemporaneously affecting an integral (e.g. x).

For instance, a Granger causal model of the form,

$$\mathbf{x}(t + \Delta t) = B_{\Delta t} \cdot \mathbf{x}(t), \quad B_{\Delta t} = \begin{pmatrix} 1 & 1 \\ 0 & 1 \end{pmatrix}, \quad (18)$$

is represented as panel (a) of Figure 5.

While, for instance, a causal model of the form,

$$\frac{d}{dt} \mathbf{x}(t) = A \mathbf{x}(t), \quad A = \begin{pmatrix} 1 & 1 \\ 0 & 1 \end{pmatrix}, \quad (19)$$

may be represented as panel (b) of Figure 5. Now, by omitting the nodes corresponding to derivatives we obtain a simplified graph G , our target for inference in this paper, as shown in panel (c) of Figure 5.

A.2 Modelling differential equations

Two-stage collocation methods were first proposed by [82]. The authors proposed to fit a smoothing estimate $\hat{\mathbf{x}}(\cdot; h, \theta)$ to the observations y_1, \dots, y_n with a smoothing parameter h , and using it and its derivative with respect to t in order to

Formulation	Example	Continuous time	Non-parametric	Irregular sampling	Free of derivative approximations	Free of cut-off values
Vector Autoregression	[12, 80]	×	✓	×	-	✓
Transfer Entropy	[73]	×	✓	×	-	×
Independence Testing	[69, 70]	×	✓	×	-	×
Two-stage collocation methods	[11, 27]	✓	×	✓	×	✓
System Identification	[8]	✓	×	✓	×	✓
Mechanistic causality	Ours	✓	✓	✓	✓	✓

Table 2: Practical comparison of models for causal discovery with data from dynamical systems.

estimate the vector field in a system of differential equations,

$$\min_{\theta} \frac{1}{n} \sum_{i=1}^n \|d\hat{\mathbf{x}}(t_i; h, \theta) - \hat{\mathbf{x}}(t_i; h, \theta)\|_2^2, \quad (20)$$

where,

$$\hat{\mathbf{x}}(\cdot; h, \theta) = \arg \min_{\mathbf{x}(\cdot; h) \in \mathcal{H}} \frac{1}{n} \sum_{i=1}^n \|\mathbf{y}_i - \mathbf{x}(t_i; h, \theta)\|_2^2. \quad (21)$$

Variations of this principle have been developed using non-linear functions of observations (e.g. see [18]), using bases of functions with out explicitly determining their form (e.g. see [11]), and using iterative methods optimizing for accurate derivatives and accurate reconstruction of the observed data (e.g. see [64]).

Using two-step collocation methods, in the broader literature, causal discovery using differential equations has been treated implicitly in physics [8] and control theory [36] where it is known as system identification; epidemiology [2, 1, 40], systems biology and pharmacology [15] where it is commonly referred to as kinetic modelling; and neuroscience [27, 26] where it is also known as dynamic causal modelling. We provide a practical contrast with some of these approaches in Table 2.

In contrast, modelling time series is of course a wide and varied research topic. One can train feed-forward or recurrent neural networks to approximate a differential equation [62]. Gaussian Processes have been adapted to fit differential equations [63] and have been proposed to model continuous-time interventions [74, 78]. Of special note are Neural ODEs [10] and many extensions that provide an elegant interface between neural networks and differential equations. The objective in these papers however is to extrapolate the latent state of the process i.e., the forward problem: inferring the latent state of the trajectory from time series. This description has not yet involved causality which, in contrast, is concerned with the inverse problem i.e., using discrete measurements of trajectories to infer the underlying causal system.

A.3 Philosophical debate about the nature of causality

A mechanistic interpretation of causality views causal claims are claims about the existence of a mechanism or process that mediates events at one time with events at a later time. Proponents of this view hold that the metaphysical connection between mechanisms and causality is very close: two events are causally connected if and only if there are connected by an underlying physical mechanism. Glennan [29, 28] and Machamer [47] define a mechanism as a *complex system* of interacting parts, but *process* accounts have also been proposed [71, 21] that focus on the fact that causal processes manifest a conserved quantity. In the latter, an interaction between two processes is causal if there is an exchange of a conserved quantity between them. Mechanistic theories of causality are normally contrasted with probabilistic [56, 79], counterfactual [67, 43, 44] and manipulationist [56, 59, 85] theories of causality. These define a connection to be causal if and only if a change in one makes a difference to the other. This distinction is a useful conceptual contrast but we should note that these accounts overlap in some measure. For instance, mechanisms can be given a counterfactual analysis and thus would be a form of difference-making theory.

Relationships between these accounts exist also in the machine learning literature. Structural equation models (the semantical framework due to Pearl [56]) have been shown to describe dynamical systems in equilibrium, and many authors have studied the meaning of interventions [52], the dependence on initial conditions [6] and the identifiability of the equilibrium causal model [17]. Some of these ideas have been extended to model dynamical systems not necessarily in equilibrium [66, 57]. The concept of local independence (a formalization of how the present of one

process depends on the past of others in a dynamical system) has also been proposed to model mechanistic causality, see e.g. [51, 23, 22, 50, 19]. In analogy to graphical Markov conditions in static data, it relates graph separation with conditional local independences across time. The difference with directed acyclic graphs is that local independence graphs allow for cycles to model feedback. Causal discovery, however, has not been considered so far to our knowledge.

B Proofs

With the notation introduced in the main body of this paper, we will use the following Lemma that extends the standard Taylor's inequality around a local optimum to unbounded sets θ^* .

Lemma 4 (Lemma 3.2. [20]) There exist $c_2, \nu > 0$ and such that $|\mathcal{R}(\theta) - \mathcal{R}(\theta_0)| \geq c_2 d(\theta, \Theta^*)^\nu$ for all $\theta \in \Theta$.

$d(\theta, \Theta^*)$ is the minimum euclidian norm between θ and any element of Θ^* .

Note also that we will use $\mathcal{R}_n(f_\theta)$ and $\mathcal{R}_n(\theta)$ interchangeably.

B.1 Proof Lemma 1

We restate the Lemma for convinience.

Lemma 1 (Generalization bound). *Assume Σ_n to be invertible and let $\alpha = (\alpha_1, \dots, \alpha_n)$ such that $\alpha_1 > \dots > \alpha_n > 0$ be its eigenvalues. For any $\delta > 0$, $\frac{n}{\|\alpha\|_2} > 3$, there exists a $C > 0$ such that,*

$$|\mathcal{R}_n(f_\theta) - \mathcal{R}(f_\theta)| \leq \left(\frac{\|\alpha\|_2}{n} \right) \sqrt{C \log \left(\frac{n}{\|\alpha\|_2} \right)}, \quad (22)$$

with probability at least $1 - \delta$.

Proof. Without loss of generality, we consider each differential equation separately. $n\mathcal{R}_n(\mathbf{f}_\theta) =: X^T X$ is a sum of dependent squared normal random variables. With this notation $X = (X_1, \dots, X_n) \in \mathbb{R}^n$ where $X_i = (Y_{ij} - \hat{x}_j(t_i)) \in \mathbb{R}$ is a univariate random variable and $Y_{ij} \in \mathbb{R}$ is the j -th random variable at time t_i given of the observation model and underlying dynamical system. $X = (X_1, \dots, X_n)$ has a joint distribution defined by a mean μ and covariance matrix Σ_n , as defined in the main body of this paper. We may write $Z = \Sigma_n^{-1/2}(X - \mu)$ and,

$$X^T X = (Z + \Sigma_n^{-1/2}\mu)^T \Sigma_n (Z + \Sigma_n^{-1/2}\mu). \quad (23)$$

Let $\Sigma_n = V^T A V$ be the eigendecomposition of Σ_n where V is an orthogonal basis of eigenvectors and A is a diagonal matrix of positive eigenvalues $\alpha = (\alpha_1, \dots, \alpha_n)$. $U = VZ$ then is also multivariate normal, with expectation zero and identity covariance matrix (since $V^T V = V V^T = I_n$). For $u = V \Sigma_n^{-1/2} \mu$, rewriting the decomposition above in terms of U and u

$$X^T X = (U + u)^T A (U + u) = \sum_{i=1}^n \alpha_i (U_i + u_i)^2. \quad (24)$$

The distribution of $n\mathcal{R}_n(\mathbf{f}_\theta) = X^T X$ is thus a weighted non-central χ^2 random variable.

Write $W = V \Sigma_n^{-1/2} \in \mathbb{R}^{n \times n}$. By applying the concentration results in Theorem 6 and 7 in [88] we have,

$$\mathbb{P}(|\mathcal{R}_n(\theta) - \mathcal{R}(\theta)| > s) \leq \exp \left\{ \frac{-C_1 n^2 s^2}{\|\alpha\|_2^2 + 2 \sum_{i=1}^n \left(\sum_{j=1}^n W_{ij} (f(x(t_j); \theta) - f(x(t_j); \theta_0)) \right)^2} \right\} \quad (25)$$

$$\leq \exp \left\{ -C_2 \left(\frac{ns}{\|\alpha\|_2} \right)^2 \right\}, \quad (26)$$

for all s such that,

$$0 < s < \frac{\|\alpha\|_2}{n \|\alpha\|_\infty} + \frac{2 \sum_{i=1}^n \left(\sum_{j=1}^n W_{ij} (f(x(t_j); \theta) - f(x(t_j); \theta_0)) \right)^2}{n}. \quad (27)$$

$C_1, C_2 > 0$ are two scalars not depending on n or α . The remaining of the proof follows the argument of [20]. We define events,

$$\mathcal{A}(\theta, s) = \{|\mathcal{R}_n(\theta) - \mathcal{R}(\theta)| > s\}, \quad (28)$$

$$\mathcal{B}(\theta, s) = \{\exists \theta' \in \Theta \text{ such that } \|\theta' - \theta\|_2 \leq \frac{s}{4M_\delta} \text{ and } |\mathcal{R}_n(\theta') - \mathcal{R}(\theta')| > s\} \quad (29)$$

$$\mathcal{C} = \{|\mathcal{R}_n(\theta) - \mathcal{R}_n(\theta')| \leq M_\delta \|\theta - \theta'\|_2, \forall \theta, \theta' \in \Theta\}, \quad (30)$$

where the last event \mathcal{C} is defined with respect to the Lipschitz constant M_δ of \mathcal{R}_n (assumed to be Lipschitz with probability at least $1 - \delta$, that is $\mathbb{P}(\mathcal{C}) \geq 1 - \delta$). Let $m = \dim(\Theta)$, there exist $C_3(m) \geq 1$ and a finite set $\mathcal{H} \subset \Theta$ such that,

$$\Theta \subset \bigcup_{\theta \in \mathcal{H}} \mathcal{V}(\theta, \epsilon), \quad |\mathcal{H}| \leq C_3/\epsilon^m, \quad (31)$$

where we choose $\epsilon = s/(4M_\delta)$. $\mathcal{V}(\theta, \epsilon)$ denotes the open ball centered at θ with radius ϵ , and $|\mathcal{H}|$ denotes the cardinality of \mathcal{H} . In other words, \mathcal{H} ϵ -covers Θ and the inequality involving the cardinality of \mathcal{H} follows because Θ is a bounded subset of Euclidian space, see e.g. section 27.1 in [75]. By a union bound over all elements in \mathcal{H} ,

$$\mathbb{P}(\exists \theta \in \mathcal{H} : |\mathcal{R}_n(\theta) - \mathcal{R}(\theta)| > s) \leq C_3(4M_\delta)^m s^{-m} \exp \left\{ -C_2 \left(\frac{n}{\|\alpha\|_2} \right)^2 s^2 \right\}. \quad (32)$$

Since $\mathcal{B}(\theta, s) \cap \mathcal{C} \subset \mathcal{A}(\theta, s)$ and $\mathcal{H} \subset \Theta$ we have,

$$\mathbb{P}(\exists \theta \in \Theta : |\mathcal{R}_n(\theta) - \mathcal{R}(\theta)| > s) \leq C_3(4M_\delta)^m s^{-m} \exp \left\{ -C_2 \left(\frac{n}{\|\alpha\|_2} \right)^2 s^2 \right\} + \delta. \quad (33)$$

Now let $k = \frac{n}{\|\alpha\|_2}$ and let $s = \frac{\sqrt{C \log(k)}}{k}$ for notational simplicity. To complete the proof we need to choose C such that,

$$C_3 \left(\frac{4M_\delta k}{\sqrt{C \log(k)}} \right)^m \exp \{ -C_2 \cdot C \cdot \log(k) \} \leq \delta. \quad (34)$$

This inequality holds if,

$$C_3(4M_\delta)^m \cdot k^{m-C_2 \cdot C} \leq \delta, \quad (35)$$

since $(C \log(k))^{m/2} \geq 1$, which can be obtained if $m - C_2 \cdot C > 0$ and $C_3(4M_\delta)^m \cdot 3^{m-C_2 \cdot C} \leq \delta$, since $k > 3$ by assumption, so that,

$$C \geq \frac{1}{C_2 \log(3)} (\log(C_3) + m \log(4M_\delta) + \log(1/\delta)). \quad (36)$$

■

B.2 Proof Lemma 2

To traverse this result, we will start by considering the converge of the group lasso.

Lemma 5 (Convergence of Group Lasso). *For any $\delta > 0$, assuming that $\lambda_{GL} \rightarrow 0$ there exists $v > 0$, $C_\delta > 0$, $N_\delta > 0$ and $T_\delta > 0$ such that,*

$$\min_{\theta \in \Theta^*} \|\hat{\theta}_n - \theta\| \leq C_\delta \left(\lambda_{AGL}^{\nu/\nu-1} + \left(\frac{\|\alpha\|_2}{n} \right) \sqrt{\log \left(\frac{n}{\|\alpha\|_2} \right)} \right)^{\frac{1}{\nu}}, \quad (37)$$

with probability at least $1 - \delta$.

Proof. Recall the group lasso and adaptive group lasso penalty terms,

$$\rho_{GL}(\theta) := \lambda_{GL} \sum_{k,j=1}^d \|[A_1^j] \cdot k\| \quad \text{and} \quad \rho_{AGL}(\theta) := \lambda_{AGL} \sum_{k,j=1}^d \frac{1}{\|[\hat{A}_1^j] \cdot k\|^\gamma} \|[A_1^j] \cdot k\|.$$

By definition, we have,

$$\mathcal{R}_n(\hat{\theta}_n) + \rho_{GL}(\hat{\theta}_n) \leq \mathcal{R}_n(\theta_0) + \rho_{GL}(\theta_0), \quad (38)$$

where $\hat{\theta}_n = \arg \min_{\theta \in \Theta} \mathcal{R}_n(\theta) + \rho_{GL}(\theta)$ is the parameter solution to the group lasso.

It holds then that,

$$\min_{\theta \in \Theta^*} c_2 \|\hat{\theta}_n - \theta\|_2^\nu \leq \mathcal{R}(\hat{\theta}_n) - \mathcal{R}(\theta_0) \quad (39)$$

$$\leq |\mathcal{R}(\hat{\theta}_n) - \mathcal{R}_n(\hat{\theta}_n)| + |\mathcal{R}(\theta_0) - \mathcal{R}_n(\theta_0)| + |\mathcal{R}_n(\hat{\theta}_n) - \mathcal{R}_n(\theta_0)| \quad (40)$$

$$\leq 2 \left(\frac{\|\alpha\|_2}{n} \right) \sqrt{C \log \left(\frac{n}{\|\alpha\|_2} \right)} + |\rho_{\text{GL}}(\theta_0) - \rho_{\text{GL}}(\hat{\theta}_n)| \quad (41)$$

$$\leq 2 \left(\frac{\|\alpha\|_2}{n} \right) \sqrt{C \log \left(\frac{n}{\|\alpha\|_2} \right)} + \lambda_{\text{GL}} \cdot K \cdot \|\theta_0 - \hat{\theta}_n\|_2, \quad (42)$$

where the first inequality is due to Lemma 4 (for some $c_2, \nu > 0$), the second inequality is due to the triangle inequality, the third inequality is due to equation (38) and Lemma 1, and the fourth inequality comes from the Lipschitzness of ρ_{GL} . We have used $K > 0$ to denote the Lipschitz constant of ρ_{GL} . The last step is given by Young's inequality, e.g. as stated in section 5.1 [20], to conclude that,

$$\min_{\theta \in \Theta^*} \|\hat{\theta}_n - \theta\|_2^\nu \leq C_\delta \left(\left(\frac{\|\alpha\|_2}{n} \right) \sqrt{\log \left(\frac{n}{\|\alpha\|_2} \right)} + \lambda_{\text{GL}}^{\frac{\nu}{\nu-1}} \right). \quad (43)$$

for some constant C_δ . ■

We will now state and prove Lemma 2.

Lemma 2 (Convergence of Adaptive Group Lasso). *For any $\delta > 0$, assuming that $\lambda_{\text{AGL}} \rightarrow 0$ there exists $v > 0, C_\delta > 0, N_\delta > 0$ and $T_\delta > 0$ such that,*

$$\min_{\theta \in \Theta^*} \|\tilde{\theta}_n - \theta\| \leq C_\delta \left(\lambda_{\text{AGL}} + \left(\frac{\|\alpha\|_2}{n} \right) \sqrt{\log \left(\frac{n}{\|\alpha\|_2} \right)} \right)^{\frac{1}{v}}, \quad (44)$$

with probability at least $1 - \delta$.

Proof. By the convergence of the group lasso $\|[\hat{A}_1^j]_{\cdot k}\|_2$ is bounded away from zero for any process k that causally significant for process $j, k, j \in \{1, \dots, d\}$. Let the set of causally significant pairs (k, j) be denoted \mathcal{S} . Then we can define,

$$\mathcal{M}(\theta) = \sum_{(k,j) \in \mathcal{S}} \frac{1}{\|[\hat{A}_1^j]_{\cdot k}\|_2^\gamma} \| [A_1^j]_{\cdot k} \|_2 < \infty. \quad (45)$$

since $\|[\hat{A}_1^j]_{\cdot k}\|_2 > 0$.

Let $\tilde{\theta}_n = \arg \min_{\theta \in \Theta} \mathcal{R}_n(\theta) + \rho_{\text{AGL}}(\theta)$ be the solution parameters of the adaptive group lasso problem. By a similar derivation to that used in (39),

$$\mathcal{R}(\tilde{\theta}_n) - \mathcal{R}(\theta_0) \leq 2C \left(\frac{\|\alpha\|_2}{n} \right) \sqrt{\log \left(\frac{n}{\|\alpha\|_2} \right)} + \lambda_{\text{AGL}} \cdot (\mathcal{M}(\tilde{\theta}_n) - \mathcal{M}(\theta_0)) \quad (46)$$

$$\leq 2C \left(\frac{\|\alpha\|_2}{n} \right) \sqrt{\log \left(\frac{n}{\|\alpha\|_2} \right)} + \lambda_{\text{AGL}} \mathcal{M}(\tilde{\theta}_n). \quad (47)$$

And since $\mathcal{M}(\tilde{\theta})$ is a finite positive scalar, again by a similar derivation to that used in (39),

$$\min_{\theta \in \Theta^*} \|\tilde{\theta}_n - \theta\|_2 \leq C_\delta \left(\left(\frac{\|\alpha\|_2}{n} \right) \sqrt{\log \left(\frac{n}{\|\alpha\|_2} \right)} + \lambda_{\text{AGL}} \right)^{1/\nu}. \quad (48)$$

for some constant $C_\delta > 0$. ■

B.3 Proof of Lemma 3

We restate the Lemma for convenience.

Lemma 3 (Causal consistency of Adaptive Group Lasso). *Let $\gamma > 0$, $\epsilon > 0$, $\nu > 0$, $\lambda_{AGL} = \Omega\left(\left(\frac{n}{\|\alpha\|_2}\right)^{-\gamma/\nu+\epsilon}\right)$, and $\lambda_{AGL} = \Omega(\lambda_{GL}^{\gamma+\epsilon})$, then the adaptive group lasso (solution to problem (8)) is causally consistent.*

Proof. By the convergence of the Group Lasso, for any pair (j, k) of non-significant processes,

$$\|[\hat{A}_1^j]_{\cdot k}\|_2 \leq C_\delta \left(\lambda_{GL}^{\nu/\nu-1} + \left(\frac{\|\alpha\|_2}{n} \right) \sqrt{\log\left(\frac{n}{\|\alpha\|_2}\right)} \right)^{\frac{1}{\nu}}, \quad (49)$$

with probability at least $1 - \delta$. It holds therefore that,

$$\lim_{\frac{n}{\|\alpha\|_2} \rightarrow \infty} \frac{1}{\|[\hat{A}_1^j]_{\cdot k}\|_2^2} \geq \infty. \quad (50)$$

Now assume for contradiction that there exists a pair (k, j) of non-causally significant processes (that is, x_k is not causally significant for x_j) such that $\|[\tilde{A}_1^j]_{\cdot k}\|_2 \neq 0$ (the \sim notation above the matrix A_1^j denotes estimation with the adaptive group lasso) and define $\phi(\tilde{\theta}_n)$ to be equal to $\tilde{\theta}_n$ except that non-significant parameters are set to zero. By the definition of $\tilde{\theta}_n$ as minimizing the empirical risk regularized by the adaptive group lasso constraint,

$$\mathcal{R}_n(\tilde{\theta}_n) + \lambda_{AGL} \frac{1}{\|[\hat{A}_1^j]_{\cdot k}\|_2^\gamma} \|[\tilde{A}_1^j]_{\cdot k}\|_2 \leq \mathcal{R}_n(\phi(\tilde{\theta}_n)). \quad (51)$$

Since the regularization term on the right-hand side is zero by the definition of $\phi(\tilde{\theta})$. Then by Assumption 3,

$$\lambda_{AGL} \frac{1}{\|[\hat{A}_1^j]_{\cdot k}\|_2^\gamma} \|[\tilde{A}_1^j]_{\cdot k}\|_2 \leq \mathcal{R}_n(\phi(\tilde{\theta}_n)) - \mathcal{R}_n(\tilde{\theta}_n) \quad (52)$$

$$\leq M_\delta \|\phi(\tilde{\theta}_n) - \tilde{\theta}_n\|_2 \quad (53)$$

$$= M_\delta \|[\tilde{A}_1^j]_{\cdot k}\|_2. \quad (54)$$

But since we have assumed $\|[\tilde{A}_1^j]_{\cdot k}\|_2 \neq 0$ it follows from above that $\lambda_{AGL} \frac{1}{\|[\hat{A}_1^j]_{\cdot k}\|_2^\gamma} \leq M_\delta$ which is a contradiction of Lemma 5 that proved the convergence of the group lasso and in particular that $\lim_{\frac{n}{\|\alpha\|_2} \rightarrow \infty} \frac{1}{\|[\hat{A}_1^j]_{\cdot k}\|_2^\gamma} = \infty$ for non-causally significant pairs of processes (k, j) . ■

C Experimental details

C.1 Results using the area under the ROC curve

In this section we report all experiments in the main body of this paper using the area under the ROC curve (AUC) as performance metric. Figure 6 contains comparisons for experiments using the Lorenz model and Table 3 contains comparisons for the Rössler and Glycolytic experiments.

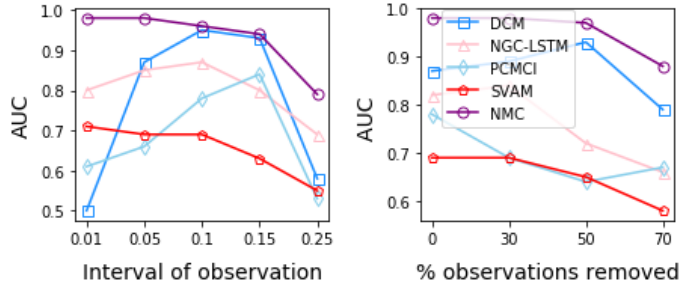


Figure 6: Experiments on Lorenz’s model.

	Rössler ($d = 10$)	Rössler ($d = 50$)	Glycolytic
NGC-MLP	.73 (.02)	.70 (.02)	.57 (.04)
NGC-LSTM	.75 (.03)	.74 (.02)	.65 (.04)
SVAM	.56 (.02)	.50 (.02)	.60 (.03)
PCMCI	.51 (.02)	.50 (.02)	.62 (.03)
DCM	.95 (.02)	.90 (.02)	.70 (.02)
NMC	.99 (.02)	.98 (.02)	.78 (.03)

Table 3: AUC on Rössler and Glycolytic data.

C.2 Purely synthetic experiment

This experiment investigates the behaviour of different regularization schemes with a purely synthetic data generating mechanism. We generate 1000 observations of 50 variables $\mathbf{X} \in \mathbb{R}^{1000 \times 50}$ using regular evaluations of the process defined by,

$$\frac{d}{dt}x_j(t) = g_j(\mathbf{x}(t)), \quad \mathbf{x}(0) = \mathbf{x}_0, \quad (55)$$

for $j = 1, \dots, 50$, where each vector field component $g_j : \mathbb{R}^{50} \rightarrow \mathbb{R}$ is parameterized by a neural network with three hidden layers of 10 nodes, such that g_j depends only on 5 (causally significant) of its 50 arguments. The initial state \mathbf{x}_0 as well as all weights and biases are independently drawn from standard Gaussian random variables before setting the causally not significant first layer columns to zero. The time interval between observations is fixed at 0.1 units.

The results are given in Table 4. We write NMC_{GL} for NMC with group lasso regularization, NMC_{AGL} for NMC with adaptive group lasso regularization and NMC_L for NMC with conventional lasso regularization. True positive rates are comparable across regularization schemes but false discovery rates are much lower for adaptive regularization which suggest that standard lasso and group lasso algorithms may not be aggressive enough to enforce sparsity strictly. As a consequence, we may need cut-off values to interpret NMC_{GL} causally which are difficult to specify in practice, while NMC_{AGL} sets most non-causal processes to zero exactly without further post-processing.

	TPR \uparrow	FDR \downarrow
NMC _L	.63 (.04)	.30 (.08)
NMC _{GL}	.71 (.05)	.25 (.08)
NMC _{AGL}	.70 (.04)	.17 (.05)

Table 4: Regularization choices.

C.3 Algorithm implementation

C.3.1 Neural Mechanistic Causality (NMC)

Proximal gradient descent. The proximal step for the group lasso penalty is given by a group soft-thresholding operation on the input weights.

In each iteration, proximal-gradient steps make two update computations to the relevant parameters, denoted here $\theta \in \{[A_1^j]_{\cdot k}, j = 1, \dots, d\}$. They are,

1. $\theta \leftarrow \theta - \alpha \nabla \mathcal{L}(\theta)$
2. $\theta \leftarrow \operatorname{argmin}_{w \in \mathbb{R}^d} \|w - \theta\|^2 + \alpha \lambda_{GL,n} \sum_{k,j=1}^d \|[A_1^j]_{\cdot k}\|$

where the second part is the proximal operator with respect to the constraint, which for each $\theta \in [A_1^j]_{\cdot k}$ is equivalent to a soft-threshold group-wise update,

$$[A_1^j]_{\cdot k} \leftarrow \frac{[A_1^j]_{\cdot k}}{\|[A_1^j]_{\cdot k}\|} \max\{0, \|[A_1^j]_{\cdot k}\| - \alpha \lambda_{GL,n}\} \quad (56)$$

Regularizing constants are chosen from the set $\{0.001, 0.01, 0.05, 0.1, 0.5, 1, 2\}$ with $\gamma = 2$ using average test errors from random train-test splits of the corresponding dataset.

Threshold selection. With this optimization procedure we do not need to set a threshold for converting the weights to the presence / absence of edges in the graph. A non-zero estimate of $\|[A_1^j]_{\cdot k}\|$ is considered as presence of an edge in the causal graph and a zero estimate of $\|[A_1^j]_{\cdot k}\|$ is considered as absence of an edge.

Architecture. The integrand f_θ was taken to be a feed-forward neural network as described with a single hidden layer of size 10 and elu activation functions after each layer except after the output layer. In each case we used the Adam optimiser as implemented by PyTorch. Starting learning rates varied between experiments (with values between 0.001 and 0.01) before being reduced by half if metrics failed to improve for a certain number of epochs. It was enough in all experiments to consider the final parameter configuration (instead of the one with best validation performance) as only norms of first layer parameters are of interest which we found not to be sensitive to the exact epoch choice. The same architecture was used for all experiments.

C.3.2 Neural Granger Causality

We implement Neural Granger Causality [80] with the code provided by the authors at <https://github.com/iancovert/Neural-GC>.

We considered two architectures: an MLP to fit the lagged time series explicitly to its next value in time, and a LSTM to model the hidden state capturing the relevant history information. We follow the author’s implementation and use a single hidden layer with 5 nodes, 5 lagged variables, relu activation function and hierarchical penalty optimized with their GISTA training procedure.

Threshold selection. NGC similarly uses an adaptive procedure to optimize parameters and presence / absence of edges in the causal graph can simply be read off as the non-zero parameters.

C.3.3 Two-stage Collocation methods (Dynamic Causal Modelling)

Two-stage collocation methods are known in the Neuroscience literature as dynamic causal models, we use this last term to denote this benchmark because dynamical causal modelling explicitly attempts to recover the causal structure. Dynamic causal modelling attempts to recover the vector field \mathbf{f} explicitly by fitting a multivariate linear model to map

the set of variables $\mathbf{X}(t) \in \mathbb{R}^d$ with estimated derivatives $d\mathbf{X}(t) \in \mathbb{R}^d$ (in our case computed separately with smoothing spline approximations).

Architecture. In our implementation, we parameterize \mathbf{f} with neural networks. We use a single hidden layer of size 10 and elu activation functions after each layer except after the output layer. In each case we used the Adam optimiser as implemented by PyTorch.

The variant of Dynamic Causal Modelling we used, with neural networks to approximate the mapping between variable states and their derivatives, is our own implementation. The architecture is similar to that used in NMC with the exception that derivatives are approximated a priori with the derivatives of natural cubic splines taken to interpolate the observed data. The smoothing hyperparameter in the spline fit was chosen for visual inspection to preserve the trajectory of the curves in each data separately.

The optimization problem thus consisted in fitting the vector field \mathbf{f}_θ explicitly such as to fit the approximated derivatives $\frac{d\mathbf{x}}{dt}(t)$ evaluated at a given time t as well as possible. Derivatives are computed from a cubic spline interpolation of the time series. We manually tune interpolation hyperparameters to obtain a visually faithful approximation of the observed trajectory for each dataset.

The optimization objective is given as,

$$\arg \min_{\mathbf{f}_\theta \in \mathcal{F}} \frac{1}{n} \sum_{i=1}^n \left\| \frac{d\mathbf{X}}{dt}(t_i) - \mathbf{f}_\theta(\mathbf{x}(t_i)) \right\|_2^2 + \rho_{\text{AGL}}(\mathbf{f}_\theta). \quad (57)$$

\mathbf{X} here denotes the interpolation over time of the time series. We use similar regularization arguments for consistency with NMC and also proximal gradient descent for optimization.

Threshold selection. For DCM, in our implementation, we use the same proximal gradient descent method with the adaptive group lasso constraint and thus we do not require a threshold to determine the presence / absence of edges in the causal graph. Presence / absence of edges is defined by non-zero parameter values.

C.3.4 PCMCI

PCMCI [68, 69, 70] is a *discrete-time* two-step approach that uses a version of the PC-algorithm with the momentary conditional independence test to account for autocorrelation in the time series.

PCMCI was implemented with the python package provided by the authors at <https://jakobrunge.github.io/tigramite/>.

Threshold selection. We chose to adjust for multiple testing with Benjamini-Hochberg’s procedure and considered associations significant, determining presence / absence of edges, with p -values below 0.00001 (chosen here because it gave a good trade-off between TPR and FDR i.e., the values with maximum F_1 score).

C.3.5 SVAM

SVAM [35] was implemented with the implementation provided by the authors at <https://github.com/cdt15/lingam> with the BIC model selection criterion and a single lagged variable. Including more lagged variables did not alter our results much but adds an additional choice as to how to define causality as we would have multiple estimated matrices of inter-relationships.

Threshold selection. We chose the threshold for converting the weights to the presence / absence of edges in the graph based on F_1 scores on validation data and was consistent (around 0.1) across datasets.

C.4 Details on Glycolysis experiment

Pharmacology is a branch of medicine that makes extensive use of dynamical models to determine the interaction patterns of drugs into the body. Like many other systems, the nonlinearity of dynamics in biology makes it hard to infer drug interactions from experimental data. Simple linear models are computationally efficient, but cannot incorporate these important nonlinearities. The glycolytic oscillator model is a standard benchmark for this kind of systems. It simulates the cycles of the metabolic pathway that breaks down glucose in cells. We simulate the system presented in Daniels and Nemenman [15] in their equation 19, mimicking glycolytic oscillations in yeast cells.

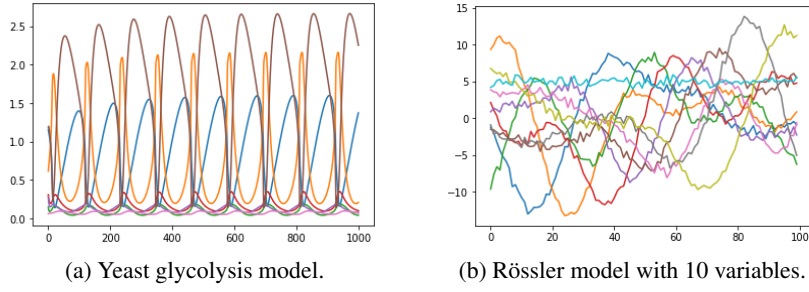


Figure 7: Sample trajectories.

The dynamics, defined by 7 biochemical components denoted x_1, x_2, \dots, x_7 , are given by the following system of equations [15],

$$\begin{aligned} \frac{d}{dt}x_1(t) &= 2.5 - \frac{100 \cdot x_1(t) \cdot x_6(t)}{1 + (x_6(t)/0.52)^4} \\ \frac{d}{dt}x_2(t) &= 2 \cdot \frac{100 \cdot x_1(t) \cdot x_6(t)}{1 + (x_6(t)/0.52)^4} - 6x_2(t) \cdot (1 - x_5(t)) - 12x_2(t)x_5(t) \\ \frac{d}{dt}x_3(t) &= 6x_2(t) \cdot (1 - x_5(t)) - 16 \cdot x_3(t) \cdot (4 - x_6(t)) \\ \frac{d}{dt}x_4(t) &= 16 \cdot x_3(t) \cdot (4 - x_6(t)) - 100 \cdot x_4(t) \cdot x_5(t) - 13 \cdot (x_4(t) - x_7(t)) \\ \frac{d}{dt}x_5(t) &= 6x_2(t) \cdot (1 - x_5(t)) - 100 \cdot x_4(t) \cdot x_5(t) - 12x_2(t)x_5(t) \\ \frac{d}{dt}x_6(t) &= -2 \cdot \frac{100 \cdot x_1(t) \cdot x_6(t)}{1 + (x_6(t)/0.52)^4} + 32 \cdot x_3(t) \cdot (4 - x_6(t)) - 1.28 \cdot x_6(t) \\ \frac{d}{dt}x_7(t) &= 1.3 \cdot (x_4(t) - x_7(t)) - 1.8 \cdot x_7(t) \end{aligned}$$

A sample of the trajectories is given in Figure 7, where after the first few time units, the system settles down onto a simple limit-cycle behavior.

As in previous examples, the system is observed over a sequence of T time points with a 0.1 time unit interval after randomly initializing each variable in the ranges provided in Table 1 of [15]. The data is stacked into two matrices for $\mathbf{X} \in \mathbb{R}^{T \times 7}$ (and $d\mathbf{X} \in \mathbb{R}^{T \times 7}$ for methods using approximated derivatives) where each row of \mathbf{X} is a snapshot of the state x in time.